

Effect of Powder-Suspended Dielectric on the EDM Characteristics of Inconel 625

Gangadharudu Talla, S. Gangopadhyay, and C.K. Biswas

(Submitted July 23, 2015; in revised form November 25, 2015; published online December 24, 2015)

The current work attempts to establish the criteria for powder material selection by investigating the influence of various powder-suspended dielectrics and machining parameters on various EDM characteristics of Inconel 625 (a nickel-based super alloy) which is nowadays regularly used in aerospace, chemical, and marine industries. The powders include aluminum (Al), graphite, and silicon (Si) that have significant variation in their thermo-physical characteristics. Results showed that powder properties like electrical conductivity, thermal conductivity, density, and hardness play a significant role in changing the machining performance and the quality of the machined surface. Among the three powders, highest material removal rate was observed for graphite powder due to its high electrical and thermal conductivities. Best surface finish and least radial overcut (ROC) were attained using Si powder. Maximum microhardness was found for Si due to its low thermal conductivity and high hardness. It is followed by graphite and aluminum powders. Addition of powder to the dielectric has increased the crater diameter due to expansion of plasma channel. Powder-mixed EDM (PMEDM) was also effective in lowering the density of surface cracks with least number of cracks obtained with graphite powder. X-ray diffraction analysis indicated possible formation of metal carbides along with grain growth phenomenon of Inconel 625 after PMEDM.

Keywords powder characteristics, powder-mixed EDM, superalloys, surface morphology, thermomechanical processing

1. Introduction

Any material that is electrically conductive can be machined using electric discharge machining (EDM). It is one of the most preferred machining processes for the manufacturing of dies, molds, and press tools. There is a great demand for high machining rate, precision, and better surface quality in the production of above-mentioned products. Powder-mixed electric discharge machining (PMEDM) is one of the recent advancements in the technology of EDM in which powder particles are added in dielectric to improve machining rate, precision, and surface quality. The suspended particles reduce overall electrical resistivity of the dielectric and allow the sparking to take place from a larger distance. The improved spark frequency and flushing conditions along with multiple sparks result in simultaneous enhancement of both material removal rate (MRR) and surface quality.

Various researchers have studied the influence of powder materials on PMEDM characteristics. Under finish machining conditions, Al powder-dispersed dielectric produced mirror finish for SKH-51 workpiece but not for SKH-54 (Ref 1). This emphasizes the importance of powder and workpiece combination in PMEDM. Dielectric with SiC powder produced higher

MRR than Al during machining of micro-slits using a horizontal copper diskette (Ref 2). It is due to the easier removal of carbon nuclides deposited on the electrode owing to high microhardness of SiC. Particle size, density, electrical conductivity, thermal conductivity, and its concentration have the most significant influence on EDM characteristics (Ref 3). Al produced the best surface finish and thinnest recast layer during PMEDM of SKD-11 mold steel using Al, Cr, Cu, and SiC powders (Ref 4). It was attributed to the combined effect of high electrical, thermal conductivities, and low density of Al. The same powder when suspended along with surfactant produced superior surface finish compared to Al alone (Ref 5). The added surfactant prevented the agglomeration of Al particles. Graphite powder resulted in higher microhardness of the machined surface compared to boric acid (H_3BO_3) due to the formation of martensite, during PMEDM of SAE 1040 steel (Ref 6). A slight decrease in surface roughness (SR) was observed when different polymer powders (Starch, PANI-emer, and PANI-salt) were added to silicone oil dielectric fluid during PMEDM of stainless steel (Ref 7). PANI-salt produced the best surface finish among the polymer powders due to its higher electrical conductivity. Among the three powders (Al, graphite, and Al_2O_3), lowest R_{max} was observed for graphite (Ref 8). Graphite easily mixes in dielectric owing to its low density. PANI-emer (polymer powder) produced finer surface finish compared to Si powder during PMEDM of stainless steel (Ref 9). Best surface quality was realized with Al, SiC, Graphite, Cr, and Fe, respectively, during EDM of γ -TiAl intermetallic. This was attributed to the combined effect of high thermal and electrical conductivities and low density of Al compared to other powder materials (Ref 10). PMEDM of various workpiece materials using different powders, tools, and dielectrics revealed the significance of powder-workpiece-tool combination for attaining desired response levels (Ref 11-14).

Process parameters like peak current, pulse-on time, duty cycle, and gap voltage were found most influential in control-

Gangadharudu Talla, S. Gangopadhyay, and C.K. Biswas, Department of Mechanical Engineering, National Institute of Technology Rourkela, Rourkela 769008, India. Contact e-mail: soumya.mech@gmail.com.

ling the response characteristics during EDM of various nickel-based super alloys (Ref 15-20). Aluminum powder, when suspended in dielectric, produced higher MRR compared to silicon powder during the PMEDM of Inconel 718 as more energy was transferred to the workpiece due to its higher thermal and electrical conductivities (Ref 21). During PMEDM of Hastelloy using aluminum powder-suspended dielectric, it was observed that MRR increased with the rise in peak current, pulse-on time, duty cycle, and gap voltage as all these contribute to the generation of high discharge energy in inter electrode gap (Ref 22). The increase in concentration of aluminum powder caused a surge in MRR due to an even distribution of heat energy over a large area during PMEDM of Inconel 718. However, too much powder concentration brought down the MRR due to agglomeration and adherence of suspended particles in the IEG. For the same reasons, SR initially declined and later climbed with powder concentration (Ref 23). Employment of cryogenically treated copper tool along with graphite impregnated dielectric resulted in reduced electrode wear ratio (EWR) (i.e., TWR/MRR). This reduction in EWR could be related to the grain refinement of tool material during the cryogenic treatment (Ref 24). Suspension of molybdenum disulfide nanopowders in dielectric during micro-drilling of Inconel 718 resulted in improvement of MRR (Ref 25). The addition of single-walled and multi-walled carbon nanotubes (CNTs) in the dielectric during PMEDM of Inconel 825 resulted in enhancement of both MRR and surface quality. The low density of CNTs prevented settling of particles at the bottom of the dielectric tank, whereas high electrical and thermal conductivities caused easy generation and distribution of discharge energy (Ref 26, 27).

Based on the previous studies, it is evident that considerable work has been reported on the role of PMEDM in improving MRR and surface finish. However, the criteria for powder material selection, based on the industrial application, are still unknown. Moreover, no significant information is also available on nickel-based super alloys that are nowadays regularly used in aerospace, chemical, and marine industries. The current research work utilized three different powders such as Al, graphite, and Si, and their role in combination with concentration and machining parameters has been evaluated on MRR, SR, radial overcut (ROC), surface hardening phenomenon,

microstructure, and possible phase changes during powder-mixed EDM of Inconel 625, for establishing selection criteria of powder material. An attempt was also made to investigate the influence of powder size and the role of impurities on PMEDM characteristics.

2. Experimental Details

A specially fabricated experimental setup was mounted on an existing die sinking EDM (model: ElektraPlusPS 50ZNC; make: Electronica, India) as shown in Fig. 1. Three different powders, i.e., aluminum, graphite, and silicon, with average particle size of $\sim 15 \mu\text{m}$, as claimed by the manufacturer (Sigma-Aldrich), were used as additives in kerosene dielectric. Electrical resistivity and thermal conductivity of powder materials are two vital properties that affect PMEDM process significantly. Electrical resistivity and thermal conductivity of pure aluminum were found to be $2.89 \mu\Omega\text{-cm}$ and $236 \text{ Wm}^{-1} \text{ K}^{-1}$ (Ref 28). Typical values of electrical resistivity and thermal conductivity for graphite powder have been reported to be $103 \mu\Omega\text{-cm}$ and $3000 \text{ Wm}^{-1} \text{ K}^{-1}$ respectively (Ref 29). Additionally, the aforesaid values for silicon powder were observed to be $2325 \mu\Omega\text{-cm}$ and $168 \text{ Wm}^{-1} \text{ K}^{-1}$ (Ref 30, 31).

Positive polarity (workpiece +ve) was used for all the experiments. Inconel 625 of rectangular shape ($40 \text{ mm} \times 40 \text{ mm} \times 5 \text{ mm}$) having chemical composition of Ni 59.27%, Cr 22.23%, Mo 8.83%, Fe 4.50%, Nb 3.5%, Mn 0.50%, Ti 0.39%, Al 0.38%, and Si 0.28% was chosen as the workpiece material. A cylindrical copper bar of 12-mm diameter was used as tool electrode.

Five process parameters, i.e., powder concentration (C_p), peak current (I_p), pulse-on time (T_{on}), duty cycle (T_{au}), and gap voltage (V_g), were selected based on previous studies. Side flushing with a pressure of 0.5 kg/cm^2 was used. A total of 32 experiments for each power were performed using central composite design of response surface methodology. Experimental ranges for all the parameters are given in Table 1. The workpiece was machined to a constant depth of 1 mm for all experimental runs.

Weight of the workpiece before and after the experiment was measured using a precision electronic balance (model: DJ

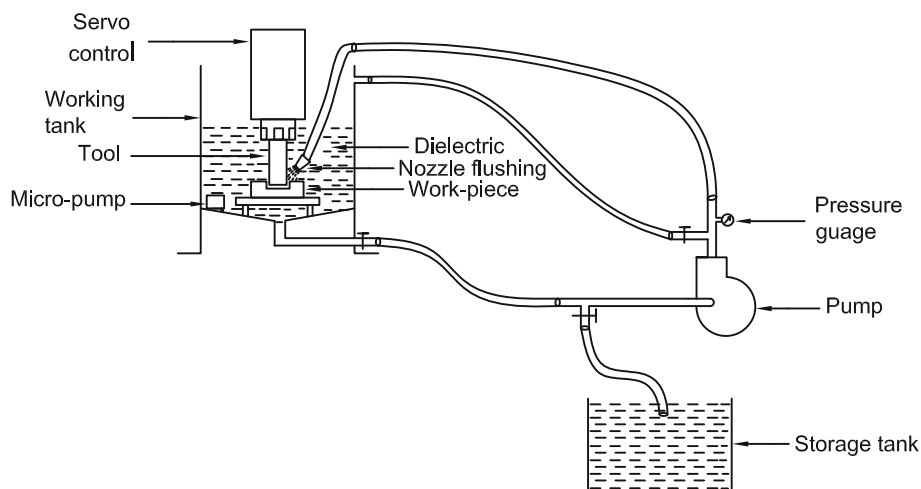
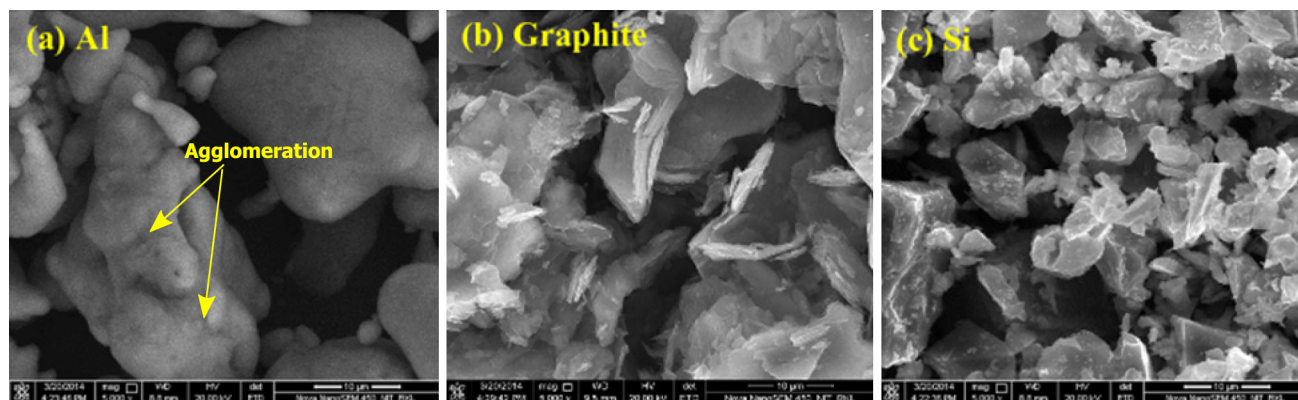


Fig. 1 Experimental setup

Table 1 Process parameters and their levels

| Parameter | Symbol | Level | | | | | Units |
|----------------------|----------|-------|-----|-----|-----|-----|---------|
| | | -2 | -1 | 0 | 1 | 2 | |
| Powder concentration | C_p | 0 | 2 | 4 | 6 | 8 | g/l |
| Peak current | I_p | 2 | 4 | 6 | 8 | 10 | A |
| Pulse time | T_{on} | 100 | 200 | 300 | 400 | 500 | μ s |
| Duty cycle | τ | 55 | 65 | 75 | 85 | 95 | % |
| Gap voltage | V_g | 40 | 50 | 60 | 70 | 80 | |

**Fig. 2** Different powder additives used in PMEDM

300S; make: Shinko Denshi, Japan; accuracy: 0.001 g) to determine MRR. The SR (R_a) of each specimen was measured at three different locations using a SR tester (model: Talysurf; make: Taylor Hobson) and mean value was taken. A tool makers microscope (make: Carl Zeiss, Germany) has been used to measure ROC. Microhardness of the machined surfaces was measured at three different places using a Vickers microhardness tester (model: LV 700; Make: Leco, USA) to present the mean values. Field emission scanning electron microscopy (FESEM) micrographs of powder particles were recorded using Nova Nanoscan 450, FEI, USA. The size distribution for different powders was measured by a particle analyzer (model: Mastersizer 2000; make: Malvern, UK). SEM (model: JSM-6084V; make: Jeol, USA) images of machined surface were taken to observe surface morphology of machined surface. Crater diameter was determined using the microscopic images that were taken by using Axiotech, 100D-3D, Carl Zeiss, Germany. X-ray diffraction (XRD) (model: Ultima IV, make: Rigaku, Japan) was carried out for identification of various phases both for powders as well as machined surface. XRD data were further utilized to determine crystallite size of the powder particles. All analyses were carried out using X'pert High score software.

3. Results and Discussion

3.1 Characterization of Different Powders

As-received aluminum, graphite, and silicon powders were characterized using various non-destructive testing methods such as scanning electron microscopy (SEM), particle size analysis, and XRD to determine the actual size, distribution,

and the presence of impurities. The results thus obtained were used to study the influence of powder size and impurities on various PMEDM characteristics of Inconel 625.

SEM micrographs of different powder additives are shown in Fig. 2. Although aluminum particles evidently have smoother surface compared to the other two, agglomeration of individual particles can also be noticed. Average size of the agglomerated particles is about $\sim 15 \mu\text{m}$, whereas the individual size might be less (3-6 μm), as observed from Fig. 1. On the other hand, graphite powder shows irregular shape with a mean size of $\sim 20 \mu\text{m}$. Silicon particles have sharp edges with irregular shape and correspond to an average size of $\sim 10 \mu\text{m}$.

The size distribution for different powders measured by a particle analyzer is shown in Fig. 3. Average sizes of graphite, silicon, and aluminum particles comprising of maximum volume of sample size are ~ 12 , ~ 16 , and $\sim 26 \mu\text{m}$ respectively. Evidently, graphite exhibits highest volume % of small particles followed by silicon and aluminum. On the other hand, aluminum indicated a small range of particle size distribution followed by silicon and graphite. One of the reasons for larger particle size measured for aluminum is the presence of extensive twinning and agglomeration in the samples (Ref 32). In this case, particle size analyzer measured the agglomerations instead of particle size.

X-ray diffraction spectra of as-received powders are demonstrated in Fig. 4. Comparison with standard XRD patterns enabled an unambiguous identification of the phases present in all three powders. The presence of oxides, i.e., Al_2O_3 and SiO_2 corresponding to (2 0 0) and (2 2 0) phases, was observed for aluminum and silicon powders, respectively. No graphite oxide (GO) (Ref 33) phase could be found for graphite powder.

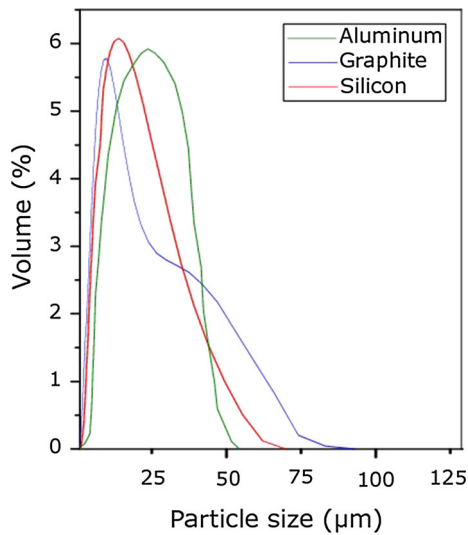


Fig. 3 Size distribution of different powders

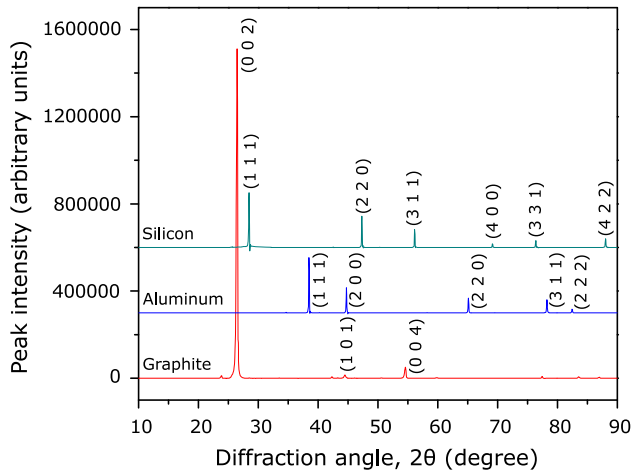


Fig. 4 XRD spectra of as-received powders

From the XRD spectra, the average crystallite sizes of the as-received powders were calculated by using Scherrer's equation (Ref 34).

$$d = \frac{K\lambda}{\beta \cos \theta}, \quad (\text{Eq 1})$$

where d is the mean crystallite size, K is the shape factor taken as 0.9, λ is the wavelength of the incident beam (1.54 Å), β is full width half maxima (FWHM), and θ is the Bragg angle. The average crystallite size of aluminum, graphite, and silicon was found to be 20, 39, and 22 nm, respectively. Apparent discrepancy in powder size might be explained by the fact that formation of particle takes place by combination of several crystallites. It may be noted that during PMEDM process, it is the particle which actually contributes to alteration in electro-physical phenomena at the discharge gap. Therefore, the size of the particle is of more relevance in the context of PMEDM process.

3.2 Material Removal Rate

For all the three powders, enhancement of MRR was observed when powder particles were uniformly dispersed in the dielectric. Such improvement in MRR can be attributed to the reduction of breakdown strength of the dielectric when conductive particles are added to it. Gap between the two electrodes increases significantly compared to conventional EDM. This increase in gap causes enlarged discharge passages. At the same time, the powder particles try to bridge the discharge gap between both the electrodes. This facilitates the dispersion of discharge into several increments resulting in increase in sparking frequency and hence, MRR increases (Ref 35).

Figure 5 shows the effect of different powder materials and process parameters on MRR. Aluminum powder produced the highest MRR followed by graphite and silicon. This is due to the lower electrical resistivity of Al (2.89 $\mu\Omega\text{-cm}$) powder compared to graphite (103 $\mu\Omega\text{-cm}$) and Si (2325 $\mu\Omega\text{-cm}$). Lower electrical resistivity of Al allows the sparking to take place from a larger distance compared to other particles leading to a rise in sparking frequency. In addition, debris is easily and quickly flushed away due to the increased spark gap. Hence, highest MRR was achieved for aluminum powder in the low concentration range (up to 6 g/l). At higher concentrations, aluminum agglomerates (as seen in Fig. 1 and 2) and the large particles adhere to workpiece leading to short circuiting and arcing. On the other hand, low density of graphite (1.26 g/cc) compared to Al (2.70 g/cc) and Si (2.33 g/cc) allows it to mix easily with the dielectric resulting in higher MRR at 8 g/l concentration. Si powder has the least electrical and thermal conductivities of the three powders. The presence of small amount of SiO_2 (Fig. 4) further reduces the electrical and thermal conductivities of Si powder. Hence, it had the least influence on MRR.

Increase in peak current leads to the rise in MRR. This is due to the increase in discharge energy. For low pulse-on time, the heating time of workpiece was so short that only a small part of material was melted, indicating that the MRR was reduced. When pulse duration is prolonged, sufficient discharge energy can be achieved, and better peak current density can be obtained. After the melted material is completely removed, a better MRR is acquired, and highly efficient impulsive force is achieved. If pulse duration is too long, the plasma channel will be so much expanded that the density of electrical discharge energy may be reduced. As a result, MRR will be diminished.

With increase in duty cycle, spark energy per pulse increased leading to higher MRR. However, at higher duty cycle, MRR decreased, due to unfavorable flushing conditions. Therefore, accumulated debris and powder particles resulted in spark short circuiting leading to arcing and unstable discharge conditions. MRR increased with gap voltage and started to decline slightly at higher values. Keeping all other parameters constant, increased gap voltage causes a hike in energy per spark leading to higher MRR. At larger gap voltage, space between electrode and workpiece becomes larger. Hence, time required to fill the IEG with neutral particles and ions is raised due the increase in gap voltage.

3.3 Surface Roughness

A considerable decrease in SR took place with the addition of conductive powder particles such as Al, graphite, and Si to

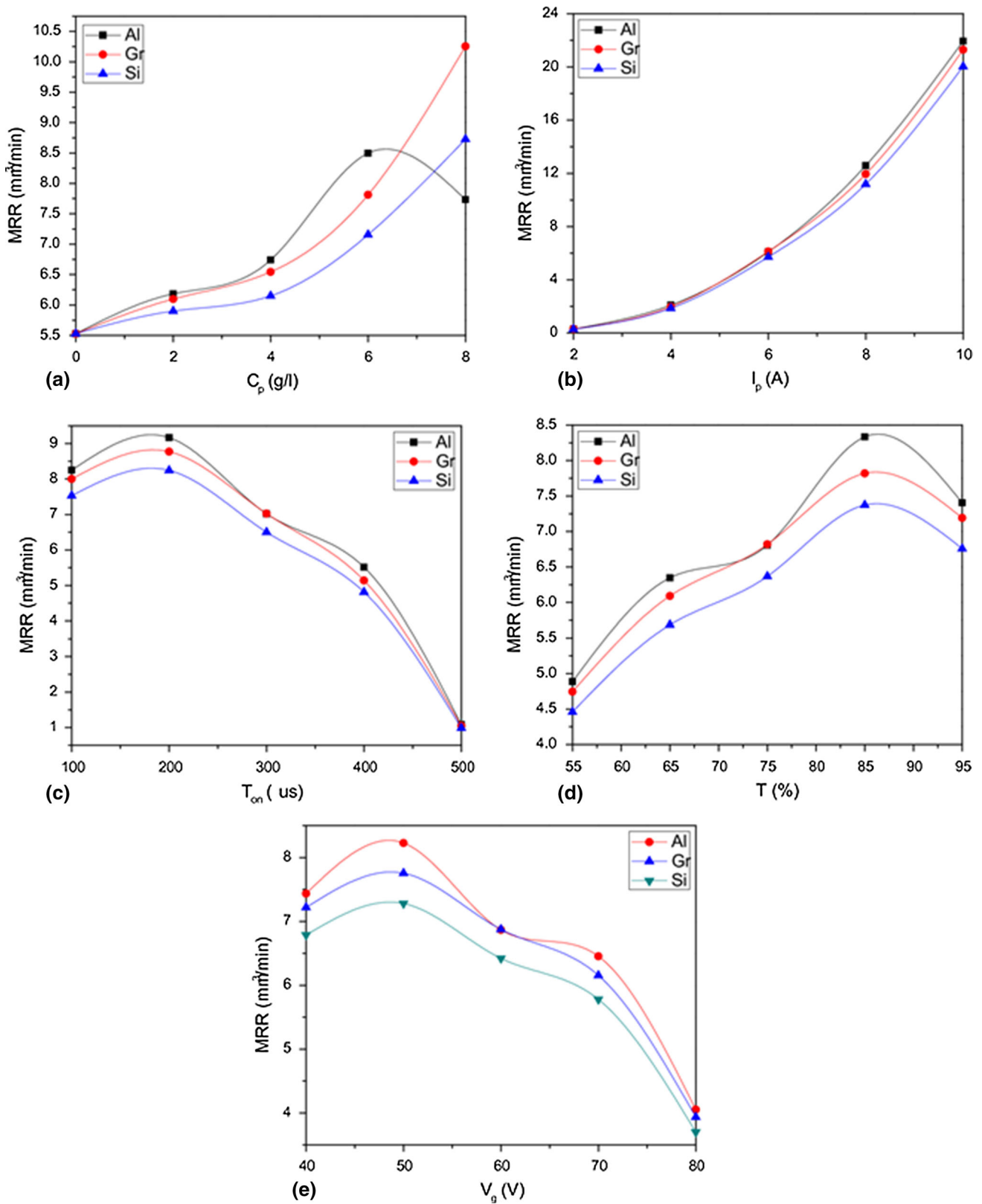


Fig. 5 Influence of process parameters on MRR

the dielectric. Plasma channel gets modified when powder particles are mixed with the dielectric. The plasma channel gets widened and enlarged. Multiple sparking among the powder

particles distributes the discharge energy over a large area. As a result, large and shallow craters are formed on the workpiece surface (Ref 4). In addition to this, the molten metal is not

heavily pressed by the plasma channel and the gas bubble. These conditions reduce the entrapping of gas in the cavities. Thus, the surface becomes less concave, smooth, and uniform (Ref 3).

Figure 6 shows the effect of different powder materials and process parameters on SR. Silicon powder produced the least SR followed by aluminum and graphite owing to its low electrical and thermal conductivities. At a given instance, more number of Si particles enter the electrode gap due to its smaller size. As a consequence, overall discharge energy is more evenly distributed in a larger area. Formation of multiple number of smaller craters during a single discharge also takes place (Ref 36). Use of smaller Si powder particles has, therefore, produced superior surface quality compared to the larger size particles of aluminum and graphite materials. The sharp edges of silicon powder as evident in Fig. 2 also augment the abrasive action of the particles on the crater edges. Thus, shallow craters are observed in case of silicon particles mixed dielectric. Although Al powder has higher electrical conductivity than graphite powder, it provides higher SR than that of graphite powder. There may be several reasons behind this behavior. First, the density of Al powder is greater than that of graphite powder, which prohibits it from mixing uniformly with the dielectric. Therefore, discharge energies are more evenly distributed among the powder particles in case of graphite powders, which make it suitable for generating smaller and shallow craters. On the other hand, the Al powder has a tendency to agglomerate owing to the electrostatic force or Van der Waals force when added to dielectric.

SR decreased with increase in powder concentration and started to decline at high concentrations. It is due to enlarged discharge heat area, which results in reduction in discharge density to form large diameter, shallow craters on the surface. The presence of excessive powder particles causes short circuiting that is responsible for the increase in SR.

Increasing the peak current increased the discharge energy and the impulsive force, removing more melted material and generating deeper and larger discharge craters resulting in high SR. SR decreased along pulse time. This may be due to dominant effect of discharge energy per pulse leading to deeper cavity and insufficient time for flushing the removed debris. SR increased with gap voltage due to the increase in discharge energy. At too long voltage values, IEG becomes very large and spark frequency reduces. This caused SR to decline.

3.4 Radial Overcut

The addition of conductive powder particles to the dielectric drastically reduces its breakdown strength. The low break down strength allows the sparking to take place from a long distance (Ref 35). Consequently, it results in increased ROC.

Figure 7 shows the effect of different powder materials and process parameters on ROC. ROC significantly varies with properties of added particles. Silicon powder had least effect on ROC. The reasons are attributed to the thermos-physical characteristics of the Si powder. Si has the highest electrical resistivity among the three powders. Therefore, among the three powder-suspended dielectrics, Si powder-suspended dielectric possesses the high insulating strength. Also, Si powder-mixed dielectric is less homogeneous compared to graphite and Al due to its high density. These two phenomena together led to a low ROC for Si powder-mixed dielectric. Al produced the largest ROC due to its high electrical conductivity.

ROC increased with increase in powder concentration. The presence of conductive or semi-conductive powders in the working gap can drastically lower the breakdown strength of dielectric, which eventually results in a higher spark gap. ROC increased along with peak current pulse time and duty cycle as well. This is due to high discharge energy. Gap voltage did not affect ROC significantly.

3.5 Microhardness

Compared to conventional EDM, more hardened surface was realized using the powder-suspended dielectric. Conductive powder particles when added to kerosene increase the ionization in IEG. The energized plasma channel causes more pyrolysis and breakage of C-H bonds. The availability of more carbon ions leads to the formation of hard metal carbides on the machined surface.

Figure 8 shows the effect of different powders and machining characteristics on microhardness (MH). Among the three powders, Si particles produced the surface with the highest MH. Among the three powders, Si produces the smallest spark gap due to its low electrical conductivity. Therefore, MH increases due to the piling up of debris in case of Si powder-mixed dielectric. In addition, less amount of heat is removed from the sparking zone owing to Si's low thermal conductivity. The presence of high amount of heat at the workpiece and quenching leads to the formation of hard surface. Formation of silicon carbide (SiC) on the machined surface also enhances the surface hardness. Silicon is followed by Al and graphite in improving the surface hardness. Higher electrical conductivity and the formation of aluminum carbide (Al_4C_3) result in harder machined surface in case of Al compared to graphite. MH improved with powder concentration as more particles enter the IEG.

MH increases with peak current due to high heating and quenching effects. MH increased with pulse time due to the increase in discharge energy. As pulse time increases, the energy density decreases and less deposition takes place. Hence, MH declines at high pulse-on time. Initial increase in duty cycle enhances MH due to increase in spark energy. At high percentage of duty cycle values, time available for cooling becomes very less. Hence, low MH values are observed. Discharge energy increases with gap voltage. At high gap voltage, the discharge gap becomes too large and heat density decreases. This causes a reduction in MH.

3.6 Surface Morphology

Microcracks on EDMed surface are developed due to thermal stresses. These cracks have deleterious impact on functional performance of machined component due to its reduced fatigue strength. In PMEDM, high thermal conductivity of the added powder takes away some part of residual heat from the sparking zone leading to drop in temperature gradient at surface and sub-surface regions. Uniform energy distribution and slow cooling rate of the molten metal due to less plasma channel pressure also reduce the formation of microcracks. Figure 9 shows the SEM images of the machined surfaces using different powder-suspended dielectrics at 8 g/l concentration. Minimum surface cracking could be observed with graphite powder due to its high thermal conductivity. It is followed by Al-suspended dielectric due to combination of high electrical and thermal conductivity. Si powder-suspended dielectric resulted in more severe thermal cracking (Fig. 9h)

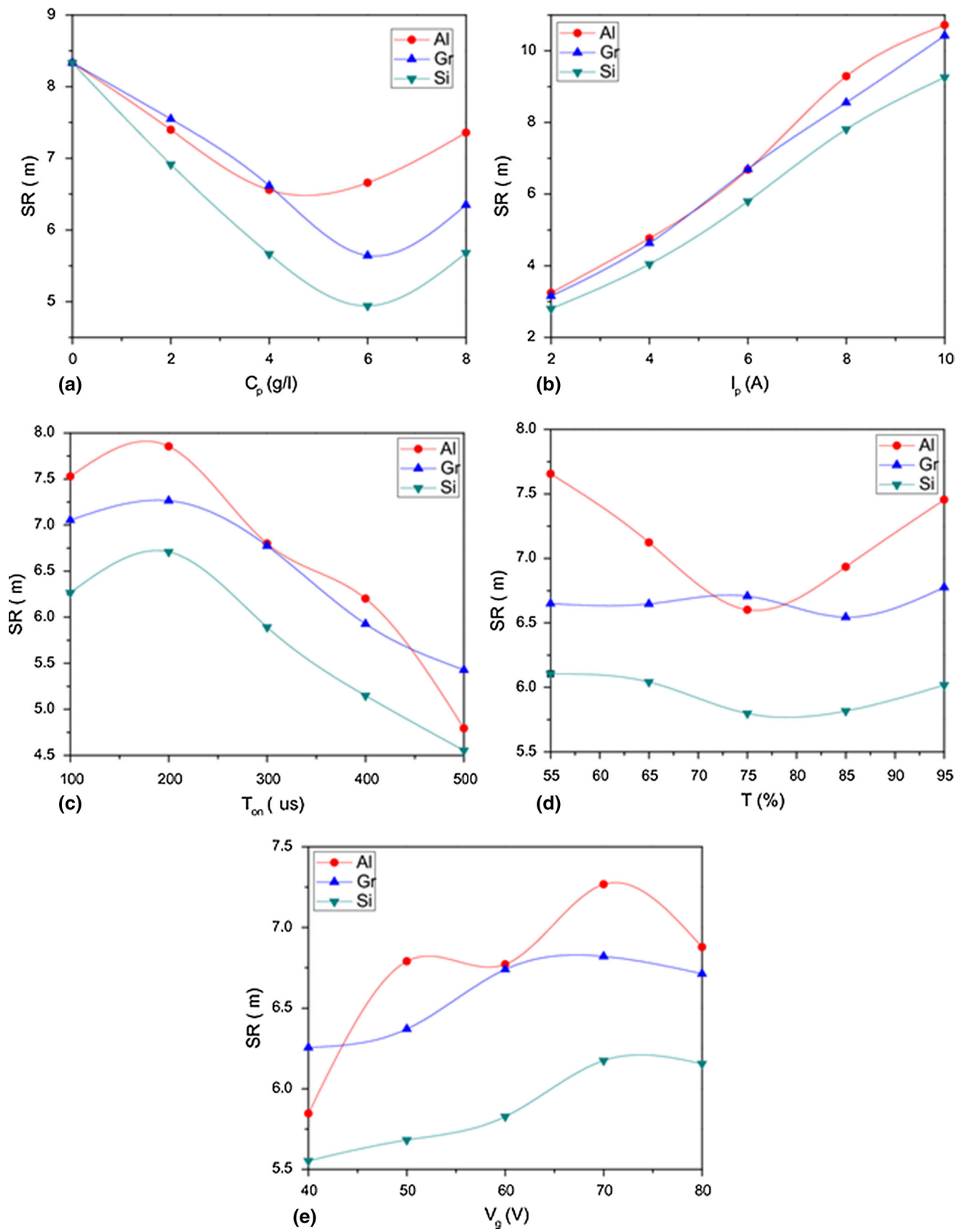


Fig. 6 Influence of process parameters on SR

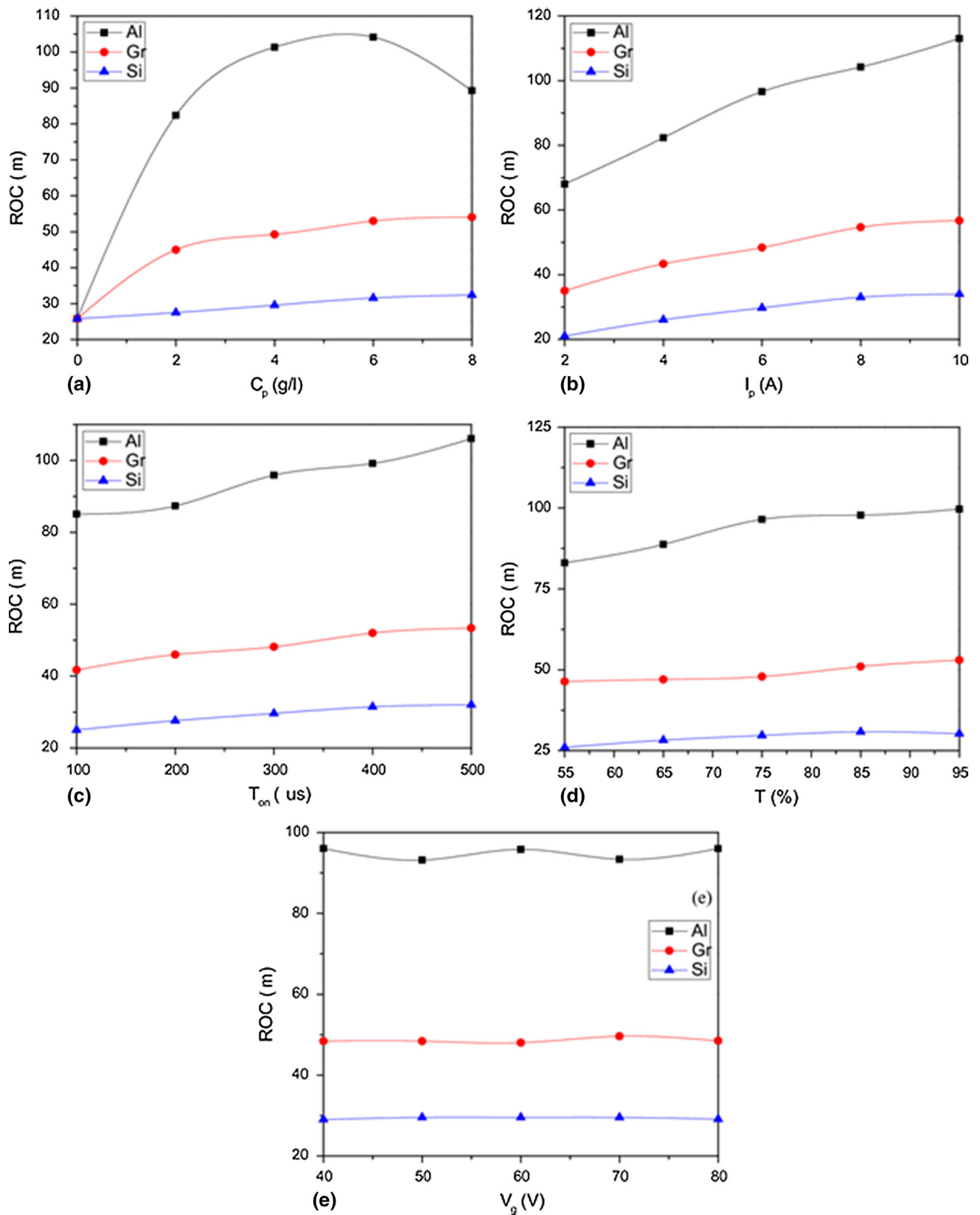


Fig. 7 Influence of process parameters on ROC

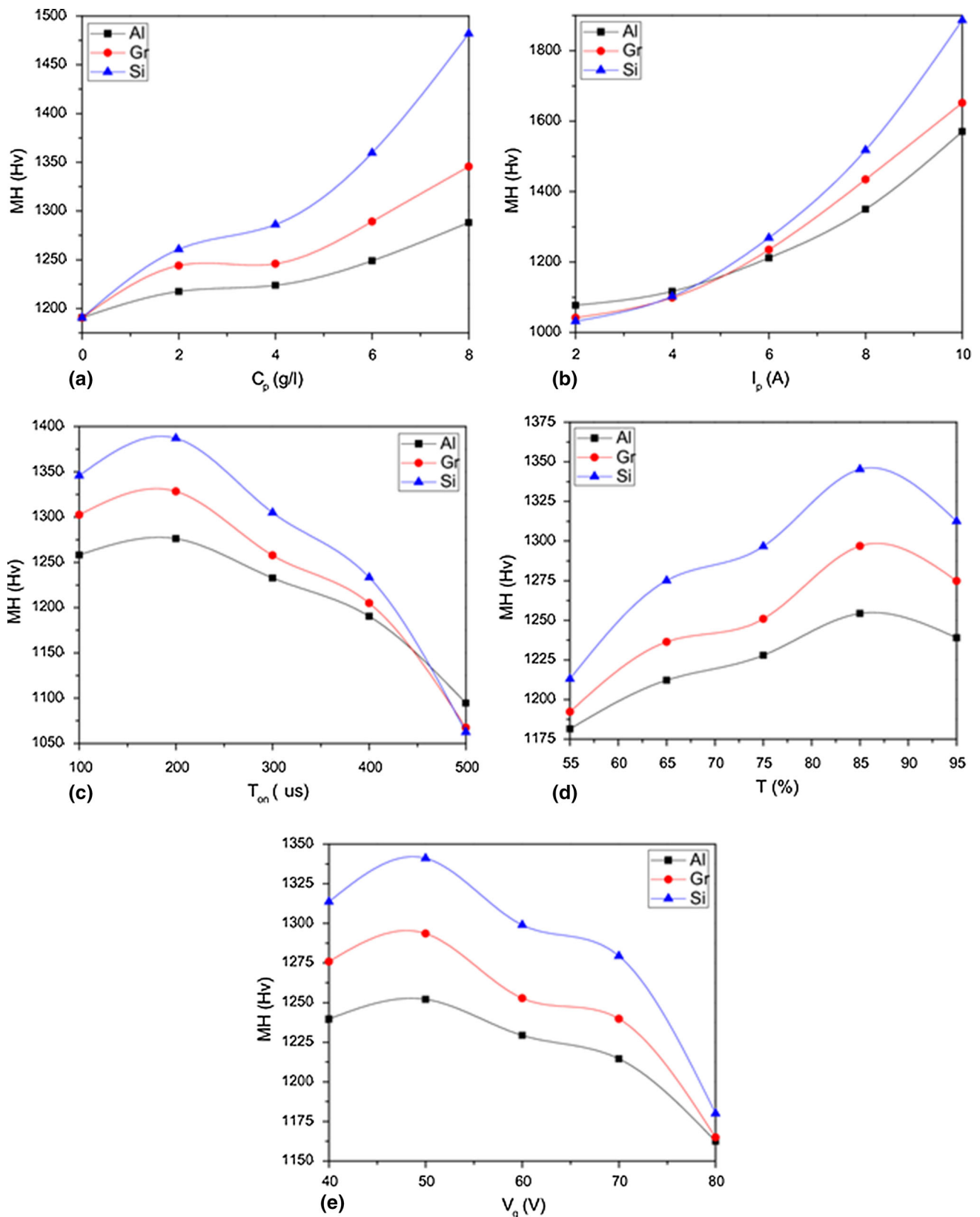


Fig. 8 Influence of process parameters on microhardness

due to its low thermal and electrical conductivities. Higher magnification images revealed the solidified globules of molten metal and pockmarks on the surface machined using conven-

tional EDM (Fig. 9b). Smooth surface with very little amount of resolidified molten metal was observed for Si powder-mixed dielectric (Fig. 9h) due to the combination of small particle size

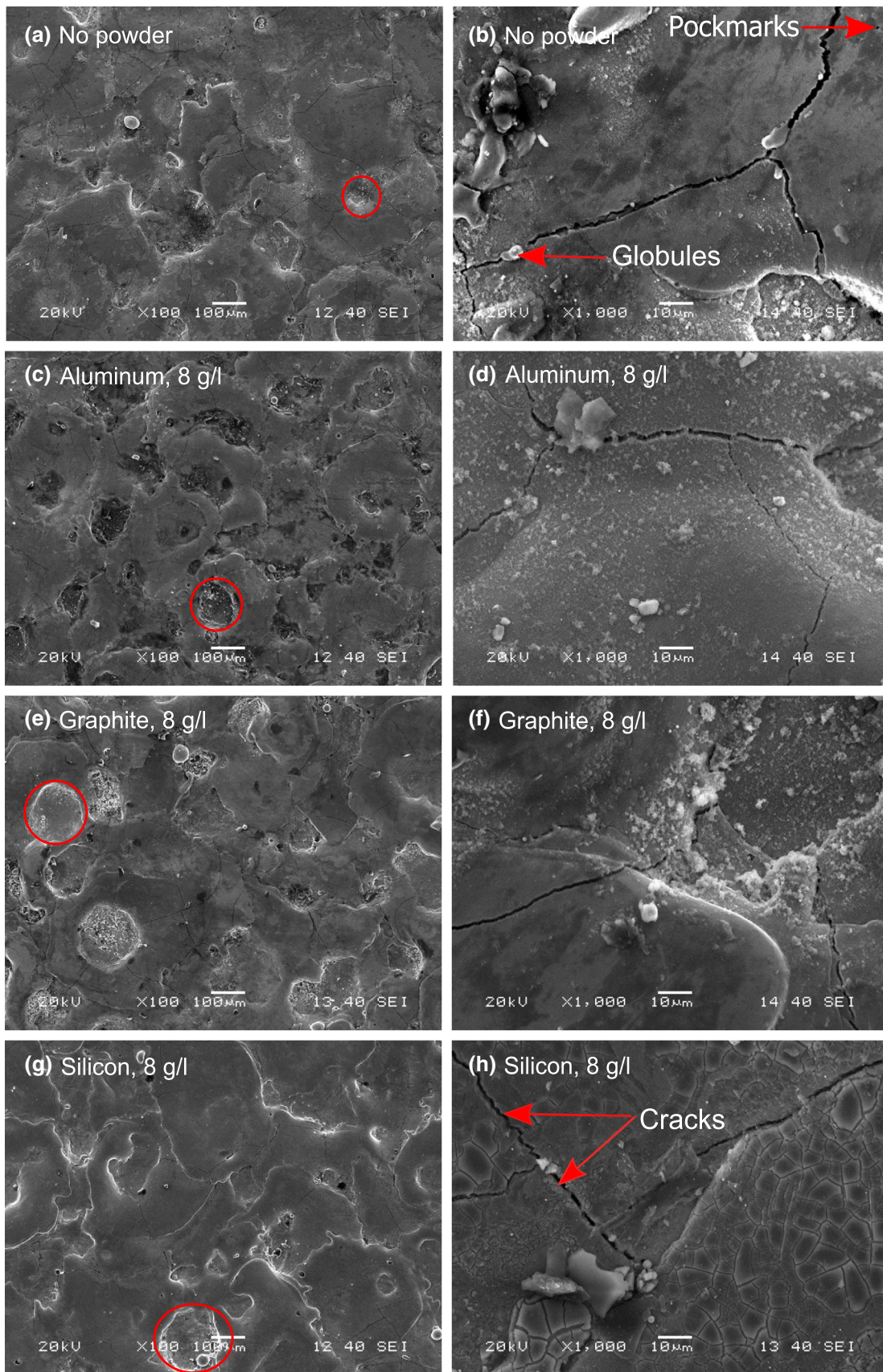


Fig. 9 SEM micrographs of machined surfaces using different dielectrics

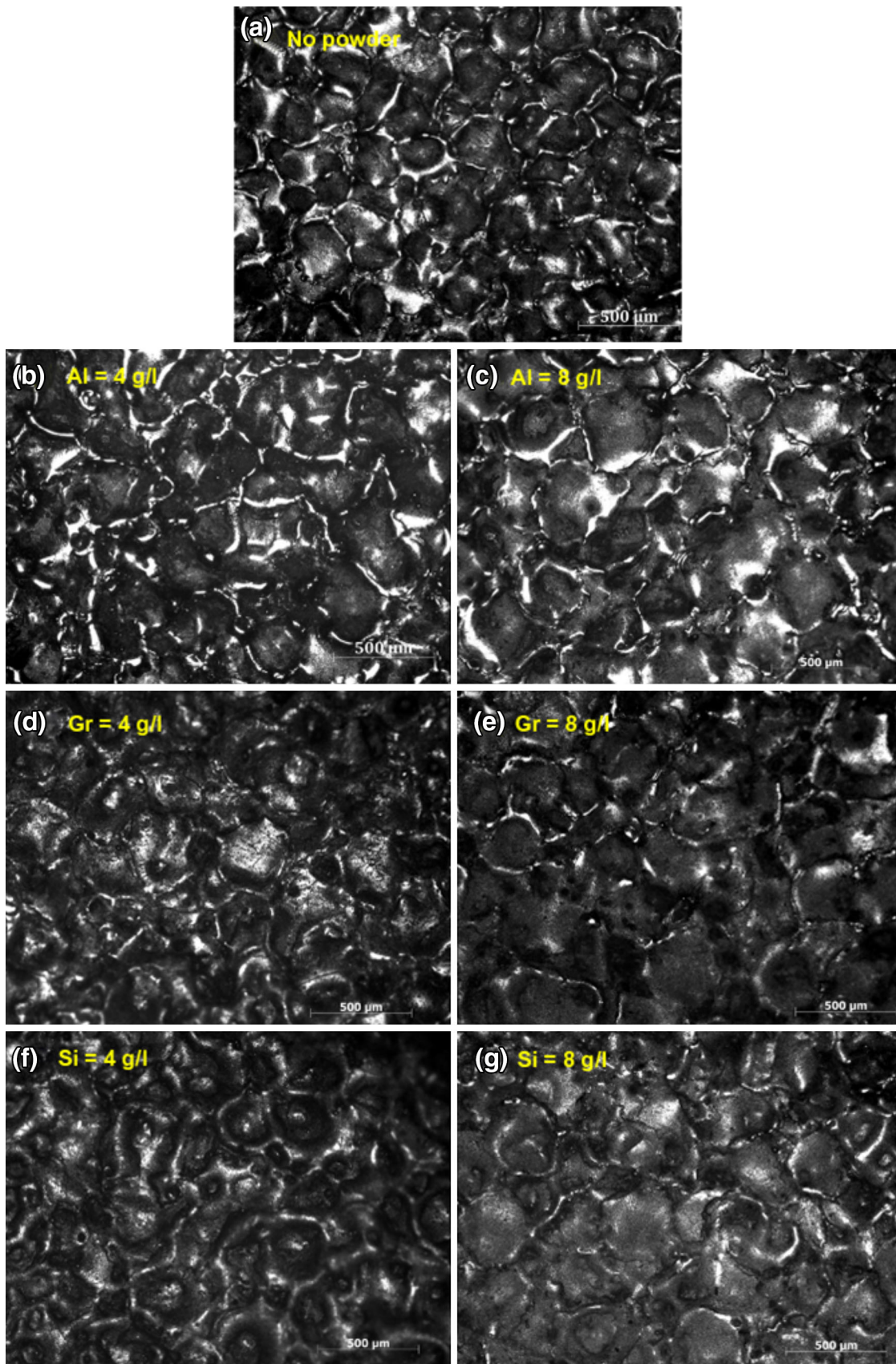


Fig. 10 Optical images showing the crater morphology of machined surfaces

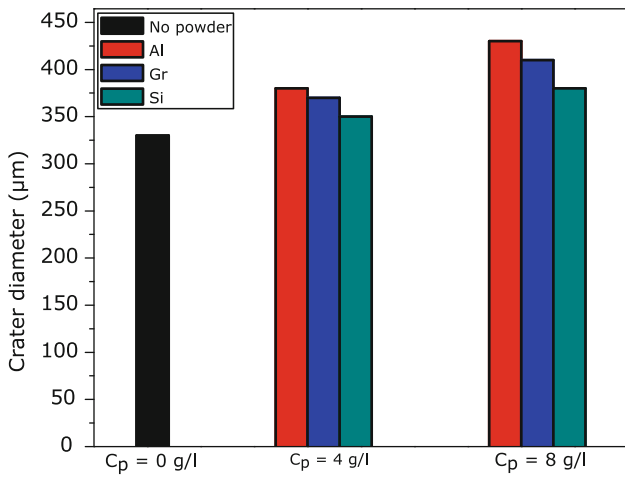


Fig. 11 Variation of crater diameter with powder concentration

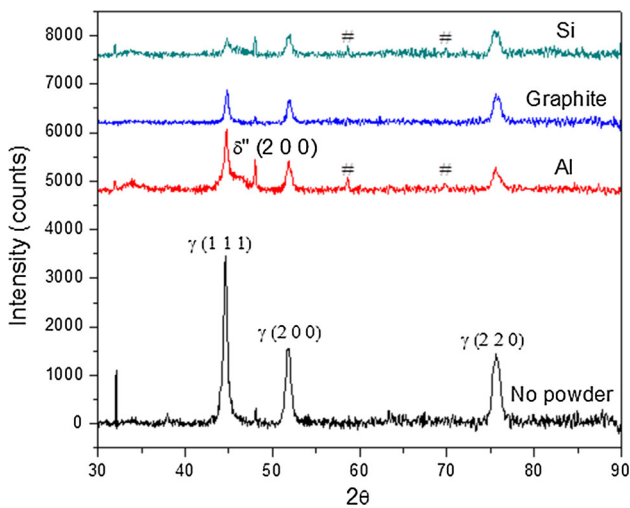


Fig. 12 XRD plots of the machined surfaces

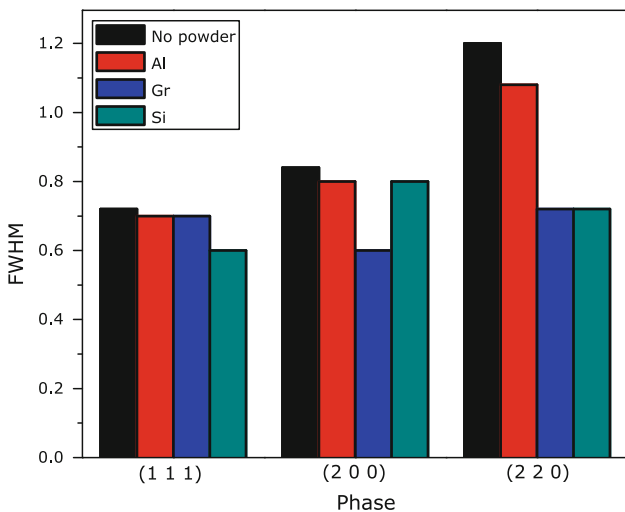


Fig. 13 FWHM for different phases in PMEDM

and abrasive action. Little consideration will also indicate that the average diameter of crater on EDMed surface without using powder-mixed dielectric is less. On the other hand, addition of powders caused average diameter to increase.

Microscopic images in Fig. 10 show the crater depth and size of the machined surface using different powder materials at varying concentrations. Deep and small craters were observed on the surface machined by conventional EDM (Fig. 9a and 10a). For all three powder-mixed dielectrics, large and shallow craters were observed compared to conventional EDM. Increase in powder concentration led to the increase in crater size. This is due to the enhanced conductivity which causes spark generation from a long distance. Enlarged IEG allows the expansion of plasma channel width. Simultaneously, external hydrostatic force acting on the plasma channel decreases. Thus, large and shallow cavities are formed on the workpiece due discharge energy spread over a larger area. Among the three powders, Al produced largest cavities as high electrical conductivity of Al allows spark to take place from a longer distance. The variation of crater diameter with powder concentration is shown in Fig. 11.

Influence of powder-mixed dielectric on crystallographic orientation of EDMed Inconel 625 has been studied using XRD technique, the spectra for which are shown in Fig. 12. While EDM with conventional dielectric primarily demonstrated fcc structure of γ -phase of Inconel 625 (Ref 37) along with some δ'' (Ni_3Al) phase, some additional peaks have been identified when Al and Si powders were added. These peaks marked by '#' in Fig. 12 indicate possible formation of carbides of Ni, Cr, and Mo from Inconel 625 apart from those of Al and Si as confirmed by X'pert High score software. Since kerosene has been used as dielectric, addition of powders caused enhanced degree of ionization as explained earlier which led to more pyrolysis which in turn might have resulted in breakage of C-H bonds. Hence, more carbon atoms would be available close to the machined surface. These metal carbides might also be responsible for surface hardening effect as evident from Fig. 8a.

Additionally, minor shift of γ (1 1 1) peak has been noted with the addition of metallic powders in dielectric fluid. This might be attributed to tensile residual stress during PMEDM process. Formation of tensile residual stress can be explained by high thermal energy associated with each discharge during PMEDM. FWHM calculated from XRD patterns have been shown in Fig. 13. It is evident that mixing of powders with dielectric caused general reduction in FWHM. This is indicative of grain growth during PMEDM which is again related to enhanced thermal energy as explained by peak shifting phenomena as well.

4. Conclusions

From the experimental investigation, it is evident that powder-mixed EDM has resulted in remarkable improvement in MRR, surface finish and surface hardening while effectively decreasing surface cracks. The role of different powders has been summarized below.

- Although indicated particle size was same for all the three powders ($\sim 15 \mu\text{m}$), detailed study clearly pointed out variation in average particle size. Aluminum exhibited lar-

gest agglomeration, while maximum volume % of finest particles was observed with graphite powder. The presence of small quantities of impurities such as SiO₂ and Al₂O₃ in as-received Si and Al powders was also ascertained.

- For low levels of powder concentration (up to 6 g/l), Al powder is recommended for achieving high MRR. However, agglomeration of Al powder at high concentration (8 g/l) led to short circuiting and arcing. Thus, at 8 g/l powder concentration, graphite powder produced the highest MRR.
- Si powder is suggested for achieving good surface finish followed by Al. Smaller size and the abrasive action of Si powder on crater edges also contributed to improvement of surface finish. However, at higher powder concentrations (above 4 g/l), graphite powder produced superior surface finish compared to Al powder.
- Least ROC was attained in conventional EDM process. However, higher degree of surface hardening could be achieved in PMEDM process. Least ROC and highest surface hardness were obtained with Si powder, followed by Al and graphite.
- Crater diameter increased with the addition of powder materials. Al produced the largest crater diameter followed by graphite and Si.
- Conventional EDM exhibited largest number of surface cracks, while PMEDM is effective in minimizing the same. Graphite is suggested for minimizing the number of surface cracks, followed by Al and Si powders.
- While conventional EDM showed typical γ and δ'' phases of Inconel 625, addition of powder in particular, Al and Si promoted formation of metal carbides. Additionally, formation of tensile residual stress and grain growth phenomena have also been indicated from XRD results.

From the experimental study, it can be concluded that Al resulted in highest MRR low powder concentrations, whereas graphite and Si yielded good results for high amounts of powder addition to the dielectric. Silicon in particular, has the potential to improve majority of surface integrity characteristics. As such, these results may aid in the proper selection of different powder materials for the desired surface modifications based on the required application.

References

1. Y.S. Wong, L.C. Lim, I. Rahuman, and W.M. Tee, Near-Mirror-Finish Phenomenon in EDM Using Powder-Mixed Dielectric, *J. Mater. Process. Technol.*, 1998, **79**, p 30–40
2. H.M. Chow, B.H. Yan, F.Y. Huang, and J.C. Huang, Study of Added Powder in Kerosene for the Micro-slit Machining of Titanium Alloy Using Electro-discharge Machining, *J. Mater. Process. Technol.*, 2000, **101**, p 95–103
3. Y.F. Tzeng and C.Y. Lee, Effects of Powder Characteristics on Electrodischarge Machining Efficiency, *Int. J. Adv. Manuf. Technol.*, 2001, **17**, p 586–592
4. T.Y. Fong and F.C. Chen, Investigation Into Some Surface Characteristics of Electrical Discharge Machined SKD-11 Using Powder-Suspension Dielectric Oil, *J. Mater. Process. Technol.*, 2005, **170**, p 385–391
5. K.L. Wu, B.H. Yan, F.Y. Huang, and S.C. Chen, Improvement of Surface Finish on SKD Steel Using Electro-Discharge Machining with Aluminum and Surfactant Added Dielectric, *Int. J. Mach. Tools Manuf.*, 2005, **45**, p 1195–1201
6. C. Cogun, B. Ozerkan, and T. Karacay, An Experimental Investigation on the Effect of Powder Mixed Dielectric on Machining Performance in Electric Discharge Machining, *Proc. Inst. Mech. Eng. Part B J. Eng. Manuf.*, 2006, **220**, p 1035–1050
7. Y.Y. Tsai and C.K. Chang, An Investigation into Surface Roughness of EDM Using Soft Particles Suspension in Silicone Oil, *Key Eng. Mater.*, 2009, **389–390**, p 430–435
8. M.P. Jahan, M. Rahman, and Y.S. Wong, Modelling and Experimental Investigation on the Effect of Nanopowder-Mixed Dielectric in Micro-electrodischarge Machining of Tungsten Carbide, *Proc. Inst. Mech. Eng. Part B J. Eng. Manuf.*, 2010, **224**, p 1725–1739
9. Y.Y. Tsai and C.K. Chang, Effects of Polymer Particles Suspending in Dielectric Fluid on Surface Roughness of EDM, *Adv. Mater. Res.*, 2010, **97–101**, p 4146–4149
10. B. Jabbaripour, M.H. Sadeghi, M.R. Shabgard, and H. Faraji, Investigating Surface Roughness, Material Removal Rate and Corrosion Resistance in PMEDM of r-TiAl Intermetallic, *J. Manuf. Process.*, 2013, **15**, p 158–166
11. A. Bhattacharya, A. Batish, and K. Singh, Fe Simulation and Experimental Validation of Powder Mixed EDM Process for Estimating the Temperature Distribution and Volume Removed in Single Crater, *Int. J. Model. Simul. Sci. Comput.*, 2012, **03**, p 1250006
12. A. Bhattacharya, A. Batish, G. Singh, and V.K. Singla, Optimal Parameter Settings for Rough and Finish Machining of Die Steels in Powder-Mixed EDM, *Int. J. Adv. Manuf. Technol.*, 2012, **61**, p 537–548
13. A. Bhattacharya and A. Batish, Effect of Process Variables on Microhardness, Grain Size and Strain During Machining of Various Die Steels with Powder-Mixed Electric-Discharge Machining Using Dummy Treated Experimental Design, *Proc. Inst. Mech. Eng. Part B J. Eng. Manuf.*, 2012, **226**, p 1192–1204
14. A. Batish and A. Bhattacharya, Mechanism of Material Deposition from Powder, Electrode and Dielectric for Surface Modification of H11 and H13 Die Steels in EDM Process, *Mater. Sci. Forum*, 2012, **701**, p 61–75
15. S.H. Kang and D.E. Kim, Investigation of EDM Characteristics of Nickel-Based Heat Resistant Alloy, *KSME Int. J.*, 2003, **17**, p 1475–1484
16. P. Kuppan, A. Rajadurai, and S. Narayanan, Influence of EDM Process Parameters in Deep Hole Drilling of Inconel 718, *Int. J. Adv. Manuf. Technol.*, 2008, **38**, p 74–84
17. V. Kumar, N. Beri, A. Kumar, and P. Singh, Some Studies on Electric Discharge Machining of Hastelloy Using Powder Metallurgy Electrode, *Int. J. Adv. Eng. Technol.*, 2010, **1**, p 16–27
18. S. Rajesha, A.K. Sharma, and P. Kumar, On Electro Discharge Machining of Inconel 718 with Hollow Tool, *J. Mater. Eng. Perform.*, 2012, **21**, p 882–891
19. A. Mohanty, G. Talla, and S. Gangopadhyay, Experimental Investigation and Analysis of EDM Characteristics of Inconel 825, *Mater. Manuf. Process.*, 2014, **29**, p 540–549
20. C.P. Mohanty, S.S. Mahapatra, and M.R.A. Singh, A Particle Swarm Approach for Multi-objective Optimization of Electrical Discharge Machining Process, *J. Intell. Manuf.*, 2014. doi:10.1007/s10845-014-0942-3
21. F. Klocke, D. Lung, G. Antonoglou, and D. Thomaidis, The Effects of Powder Suspended Dielectrics on the Thermal Influenced Zone by Electrodischarge Machining with Small Discharge Energies, *J. Mater. Process. Technol.*, 2004, **149**, p 191–197
22. P. Singh, A. Kumar, N. Beri, and V. Kumar, Influence of Electrical Parameters in Powder Mixed Electric Discharge Machining (PMEDM) of Hastelloy, *J. Eng. Res. Stud.*, 2010, **1**, p 93–105
23. A. Kumar, S. Maheshwari, C. Sharma, and N. Beri, Analysis of Machining Characteristics in Additive Mixed Electric Discharge Machining of Nickel-Based Super Alloy Inconel 718, *Mater. Manuf. Process.*, 2011, **26**, p 1011–1018
24. A. Kumar, S. Maheshwari, C. Sharma, and N. Beri, Machining Efficiency Evaluation of Cryogenically Treated Copper Electrode in Additive Mixed EDM, *Mater. Manuf. Process.*, 2012, **27**, p 1051–1058
25. G.S. Prihandana et al., Application of Powder Suspended in Dielectric Fluid for Fine Finish Micro-EDM of Inconel 718, *Int. J. Adv. Manuf. Technol.*, 2014, **75**, p 599–613

26. S. Prabhu and B.K. Vinayagam, AFM Surface Investigation of Inconel 825 with Multi Wall Carbon Nano Tube in Electrical Discharge Machining Process Using Taguchi Analysis, *Arch. Civ. Mech. Eng.*, 2011, **11**, p 149–170
27. S. Prabhu and B.K. Vinayagam, AFM Nano Analysis of Inconel 825 with Single Wall Carbon Nano Tube in Die Sinking EDM Process Using Taguchi Analysis, *Arab. J. Sci. Eng.*, 2013, **38**, p 1599–1613
28. R. Brandt and G. Neuer, Electrical Resistivity and Thermal Conductivity of Pure Aluminum and Aluminum Alloys up to and Above the Melting Temperature, *Int. J. Thermophys.*, 2007, **28**, p 1429–1446
29. A.C. Wilson and W.W. Tyler, Thermal Conductivity, Electrical Resistivity, and The thermoelectric Power of Graphite, *Phys. Rev.*, 1953, **89**, p 870–875
30. W. Fulkerson, J.P. Moore, R.K. Williams, R.S. Graves, and D.L. McElroy, Thermal Conductivity, Electrical Resistivity, and Seebeck Coefficient of Silicon from 100 to 1300 K, *Phys. Rev.*, 1968, **167**, p 765–782
31. H.R. Shanks, P.D. Maycock, P.H. Sidles, and G.C. Danielson, Thermal Conductivity of Silicon from 300 to 1400 K, *Phys. Rev.*, 1963, **130**, p 1743–1748
32. Y. Du, H. Chen, R. Chen, and N. Xu, Synthesis of p-Aminophenol from p-Nitrophenol Over Nano-sized Nickel Catalysts, *Appl. Catal. A. Gen.*, 2004, **277**, p 259–264
33. G.I. Titelman, V. Gelman, S. Bron, R.L. Khalfin, Y. Cohen, and H. Bianco-Peled, Characteristics and Microstructure of Aqueous Colloidal Dispersions of Graphite Oxide, *Carbon N Y*, 2005, **43**, p 641–649
34. A. Patterson, The Scherrer Formula for X-Ray Particle Size Determination, *Phys. Rev.*, 1939, **56**, p 978–982
35. H.K. Kansal, S. Singh, and P. Kumar, Effect of Silicon Powder Mixed EDM on Machining Rate of AISI, D2 Die Steel, *J. Manuf. Process.*, 2007, **9**, p 13–22
36. K.Y. Kung, J.T. Horng, and K.T. Chiang, Material Removal Rate and Electrode Wear Ratio Study on the Powder Mixed Electrical Discharge Machining of Cobalt-Bonded Tungsten Carbide, *Int. J. Adv. Manuf. Technol.*, 2009, **40**, p 95–104
37. M. Shakil et al., Microstructure and Hardness Studies of Electron Beam Welded Inconel 625 and Stainless Steel 304L, *Vacuum*, 2014, **110**, p 121–126